40th AIAA/ASME/SAE/ASEE Joint Propulsion Conference and Exhibit
11 - 14 July 2004, Fort Lauderdale, Florida

AIAA 2004-4132

LES of Supersonic Combustion of Hydrocarbon Spray in a SCRAMJET

F. Génin* and S. Menon†
School of Aerospace Engineering
Georgia Institute of Technology
Atlanta, Georgia 30332

Large Eddy Simulation (LES) of a liquid hydrocarbon-fueled SCRAMJET engine that corresponds to an experimental facility is carried out here to investigate the nature of spray mixing and combustion in this configuration. The mixing efficiency of two different injection strategies is first studied with a particular focus on the interaction of the spray and the vaporized fuel with the shear layer that forms at the rearward facing flame holder. It appears that better flame-holding characteristics are achieved when injection is performed just upstream the cavity leading-edge. The mass addition into the shear layer tends to increase the mixing properties of this configuration. Simulation of a reacting flow for the latter injection strategy is then performed. A particular emphasis is placed upon the issues of ignition in high-speed dual-phase flow. Characteristic flow features and limitations of this injection approach are examined.

Nomenclature

CFD	Computational Fluid Dynamics
LES	Large Eddy Simulation
$RANS$	Reynolds-Averaged Navier Stokes Simulation
$\bar{\Delta}$	Local grid size
ρ	density
u_i	Velocity in the ith-direction
x_i	Cartesian body axes
p	Pressure
τ	Stress terms
F	Coupling force
e	Sensible Energy
h	Sensible Enthalpy
σ	Viscous Work
D	Dissipation
Q	Energy source term
Y_k	Species Mass fraction
V	Diffusion Velocity
w	Chemistry source term for the species
S	Spray source term for the species
c_p	Specific heat for constant pressure
c_v	Specific heat for constant volume
κ	Thermal conductivity
ν	Dynamic viscosity
F_k	Spray source term for the turbulent kinetic energy
n	number of droplets per group
m	mass of a droplet
V	Droplet velocity
r	droplet radius
Re	Reynolds number
Pr	Prandtl number
B	Spalding number
C_D	Drag Coefficient

Subscripts

s	spray
C	Combustion
t	Turbulent quantity
d	Droplet
i	space index (1,2,3)
k	species index
f	fuel

Superscripts

sgs	Subgrid Scale

Overheads

$\overline{X}$	volume averaged
$\widetilde{X}$	Favre averaged
$\dot{X}$	rate of change

1 Introduction

The successful development of SCRAMJET engines is essential for the development Single-stage-to-orbit (SSTO) space planes, as well as for hypersonic aircrafts. While most of the earlier works were focused on gaseous hydrogen fueled engines, a significant interest has recently been focused toward the use of hydrocarbon fuels in SCRAMJET applications (see, for example[1, 2]). It has been shown,[3] that for a flight Mach number below 9-10, hydrocarbon fuels present a viable alternative to hydrogen. The advantage of higher specific heat of hydrogen fuel is negated by its low density and the necessity for storage at cryogenic temperature. Hydrocarbon fuels, on the other hand, allow significant simplification of fuel system, operational procedure and provide increased safety. They

*AIAA Student Member, Graduate Research Assistant
†AIAA Associate Fellow, Professor

also benefit from an extensive design, manufacturing and maintenance experience accumulated by aircraft and missile industry.

An important issue which needs to be addressed in SCRAMJET design is mixing enhancement since it is an essential element for the success or failure of supersonic combustion. Fuel-air mixing is complicated by a variety of physical and geometrical constraints. For example, increase in the effective convective Mach number[4] reduces the growth of shear layers and hence inhibits mixing. Geometry constraints mixing as well since the dimensions of the combustor cannot be adjusted to increase mixing. On the other hand, fuel-air mixing could be enhanced by modifying the injection process, e.g., ramped injectors,[5] by creating secondary (3D) instability in the shear layer[6] and/or by shock induced shear layer mixing.[7] All these methods have their advantages and disadvantages and an optimal procedure applicable to various combustor Mach number is still not available.

The above issues are even more complicated when liquid fuel is employed since fuel spray vaporization time-scale introduces another variable into the mixing process. Earlier experimental studies at WPAFB[8] showed that hydrocarbon combustion at a Mach number of 2.1 can be achieved by using a ramped cavity but only when the liquid fuel is preheated to crack the fuel and to create gaseous hydrocarbons. Fuel-air mixing and combustion when a liquid fuel if injected as is (i.e., as a spray) are not properly understood at this time.

Due to the complexity of the physics involved in SCRAMJET combustion and the difficulties in experimental investigation of such processes, simulations are expected to play an ever increasing role in the design process. In addition to access to flow conditions and flow features which can not be readily obtained experimentally, CFD can greatly reduce the length and cost of the design cycle, due to the continuous advances in computer technology and the development of more sophisticated flow simulation software.

However, conventional CFD techniques such as Reynolds-Averaged Navier Stokes (RANS) approaches have failed in the past to resolve many of the issues related to SCRAMJET fuel-air mixing, since this is primarily an unsteady phenomenon. A promising technique for predicting the effects of turbulence in flows of technological interest is Large Eddy Simulation (LES).[9,10] In LES, all scales larger than the grid is modeled using a space and time accurate scheme and only the small scales are modeled using a subgrid model that is considered relatively universal. The direct computation of the large, energy-containing eddies (which are geometry and flow dependent features) gives LES more generality than the RANS. The computational cost of LES, although significant is fast becoming reasonable on massively parallel computers, especially on PC based Linux clusters.

This paper reports on some recent LES studies of mixing and combustion of hydrocarbon liquid fuel in the flow field over a ramped cavity. The configuration adopted, as well as the inflow conditions, correspond as much as possible to the actual facility and the test conditions in the AFRL/PRSC Supersonic Combustion Research Facility.[11,12,8] The influence of the injector location, and of the droplet size distribution on the mixing, dynamics of the flow, and on the combustion efficiency is investigated.

2 Formulation

2.1 LES Governing Equations

The governing equations for LES are obtained by applying a spatial filter (based on the local grid size $\overline{\Delta}$) to the compressible Navier-Stokes equations for the mass, momentum, internal energy, and species conservation. Favre averaging, commonly used in the study of compressible flow, is defined by $\widetilde{f} = \overline{\rho f}/\overline{\rho}$, where the over-line stands for volume averaging. The resulting equations are given by:

$$\begin{cases} \frac{\partial \overline{\rho}}{\partial t} + \frac{\partial \overline{\rho} \widetilde{u_i}}{\partial x_i} = \widetilde{\dot{\rho}_s} \\ \frac{\partial \overline{\rho} \widetilde{u_i}}{\partial t} + \frac{\partial}{\partial x_j}\left[\overline{\rho}\widetilde{u_i}\widetilde{u_j} + \overline{p}\delta_{ij} - \overline{\tau_{ij}} + \tau_{ij}^{sgs}\right] = \widetilde{\dot{F}_{s,i}} \\ \frac{\partial \overline{\rho} \widetilde{e}}{\partial t} + \frac{\partial}{\partial x_i}\left[\left(\overline{\rho}\widetilde{e} + \overline{p}\right)\widetilde{u_i} + \overline{q_i} + h_i^{sgs} - \widetilde{u_j}\tau_{ji}^{sgs} + \sigma_i^{sgs}\right] \\ \qquad = \widetilde{u_i}\frac{\partial \overline{p}}{\partial x_i} + \overline{\tau_{ij}}\frac{\partial \widetilde{u_i}}{\partial x_j} + D^{sgs} + \overline{\dot{Q}_c} + \widetilde{\dot{Q}_s} \\ \frac{\partial \bar{\rho}\tilde{Y}_k}{\partial t} + \frac{\partial}{\partial x_i}[\bar{\rho}\tilde{Y}_k\tilde{u}_i - \bar{\rho}\tilde{Y}_k\widetilde{V_{i,k}} + Y_{i,k}^{sgs} + \theta_{i,k}^{sgs}] = \\ \qquad \bar{\dot{w}}_k + \widetilde{\dot{S}_{s,k}} \qquad k = 1, N_s \end{cases} \tag{1}$$

where $\overline{\dot{\rho}^s}$, $\overline{F_i^s}$, $\overline{\dot{Q}^s}$ and $\widetilde{\dot{S}_{s,k}}$ are respectively, the source terms from the spray evaporation for mass, momentum, energy, and species (these terms will be explicitly described in 2.2), and $\overline{\dot{Q}_c}$ and $\bar{\dot{w}}_k$ are source terms from the chemistry.

The quantity $\widetilde{e}$ is the filtered internal sensible energy, computed as $\tilde{e} = \sum_{k=1}^{N_s}[c_{v,k}\tilde{Y}_k\tilde{T}]$. A transport equation for the internal sensible energy rather than for the total energy, is adopted here for supersonic flows since the amount of kinetic energy in total energy is very large and dominates the budget of the total energy equation. Consequently, numerical errors in internal energy can be significant.

Perfect gas is assumed, with a constant specific heats ratio of 1.4. Both the viscosity and the thermal conductivity of the species were approximated by a Sutherland law. The heat flux term is written in the following form:

$$\bar{q}_i = -\bar{\kappa}\frac{\partial \tilde{T}}{\partial x_i} + \bar{\rho}\sum_{k=1}^{N_s}\tilde{h}_k\tilde{Y}_k\widetilde{V_{i,k}}.$$

The diffusion velocities are approximated using Fickian diffusion as $\widetilde{V_{i,k}} = (-\bar{D}_k/\tilde{Y}_k)(\partial \tilde{Y}_k/\partial x_i)$ where

pressure diffusion (Dufour) and temperature diffusion (Soret) effects are neglected.

Several terms in the LES equations require closure. Here, a closure based on a transport model for the subgrid kinetic energy k^{sgs} is used to close the momentum and energy subgrid fluxes. In this approach, a one-equation model for k^{sgs}:

$$\frac{\partial \overline{\rho} k^{sgs}}{\partial t} + \frac{\partial}{\partial x_i}(\overline{\rho}\widetilde{u_i}k^{sgs}) = P^{sgs} - D^{sgs} + \frac{\partial}{\partial x_i}\Big(\frac{\overline{\rho}\nu_t}{Pr_t}\frac{\partial k^{sgs}}{\partial x_i}\Big) + F_k \quad (2)$$

is solved along with the LES equations. Here, F_k is the work done due to the two-phase coupling force term $\dot{F_{s,i}}$. This term is defined in 2.2. ν_t is the turbulent viscosity and Pr_t is the turbulent Prandtl number. ν_t, the turbulent viscosity, P^{sgs}, the subgrid kinetic energy production and D^{sgs}, the subgrid kinetic energy dissipation, are given by:

$$\nu_t = C_\nu \sqrt{k^{sgs}}\ \overline{\Delta} \quad (3)$$

$$P^{sgs} = -\tau_{ij}^{sgs}\frac{\partial \widetilde{u_i}}{\partial x_j} \quad (4)$$

$$D^{sgs} = C_\epsilon \overline{\rho}\frac{\sqrt{(k^{sgs})^3}}{\overline{\Delta}} \quad (5)$$

The subgrid stresses and energy flux are then closed as follows:

$$\tau_{ij}^{sgs} = -2\overline{\rho}\nu_t\big(\widetilde{S_{ij}} - \frac{1}{3}\widetilde{S_{kk}}\delta_{ij}\big) + \frac{2}{3}\overline{\rho}k^{sgs}\delta_{ij} \quad (6)$$

$$h_i^{sgs} = -\overline{\rho}\frac{\nu_t}{Pr_t}\frac{\partial \widetilde{h}}{\partial x_i} \quad (7)$$

where $\widetilde{h}$ is the sensible enthalpy. The subgrid viscous work, σ_i^{sgs}, that appears in the filtered energy equation, is neglected, based on the earlier work of Kim *et al.*[13] In the above closure, two model coefficients C_ν and C_ϵ appear. Currently, we employ constant values of 0.067 and 0.916 for these constants based on earlier evaluation of these parameters.[14] A localized dynamic approach (LDKM) has also been developed[15] to compute these coefficients as a part of the solution. This approach is currently under evaluation for supersonic combustion,[16] and is used here for a non-reacting mixing case in the present study.

2.2 Continuum/Dispersed Phase Coupling

The volume averaged inter-phase source terms that appear on the right hand side of the LES equations (1) are given by:[17]

$$\dot{\rho}_s = [-\rho_d\frac{dV_d}{dt} + V_d\frac{d\rho_d}{dt}]$$

$$\dot{F}_{s,i} = [(-\rho_d\frac{dV_d}{dt} + V_d\frac{d\rho_d}{dt})u_{i,d} + \rho_d V_d\frac{du_{i,d}}{dt}]$$

$$\dot{Q}_s = [(-\rho_d\frac{dV_d}{dt} + V_d\frac{d\rho_d}{dt})e_{t,d} + \rho_d V_d\frac{de_{t,d}}{dt}]$$

$$\dot{S}_{s,k} = [(-\rho_d\frac{dV_d}{dt} + V_d\frac{d\rho_d}{dt})Y_{k,d} + \rho_d V_d\frac{dY_{k,d}}{dt}]$$

These terms are computed as follows:[18,19]

$$\begin{pmatrix} \widetilde{\dot{\rho}_s} \\ \widetilde{\dot{F}_{s,i}} \\ \widetilde{\dot{Q}_s} \\ \widetilde{\dot{S}_{s,k}} \end{pmatrix} = \begin{pmatrix} \sum_m n_d\dot{m}_d \\ \sum_m n_d\dot{m}_d u_{i,d} - \frac{4\pi}{3}\rho_d r_d^2 n_d\frac{du_{i,d}}{dt} \\ \sum_m n_d\dot{m}_d h_{fs} - 4\pi r_d^2 n_d h\Delta T \\ \sum_m n_d\dot{m}_d \end{pmatrix}$$

In all the expressions that follow, subscript d refers to droplet quantities. Here, ρ_d, V_d, $u_{i,d}$, $e_{t,d}$, and $Y_{k,d}$ are the density, volume, "i-th" component of the velocity, total energy and species mass fraction of the droplets, respectively and n_d is the number of droplets in a group. The summation index "m" is over all the droplets crossing a LES cell volume. The influence of the liquid phase on the k^{sgs} transport equation is modeled as:

$$F_k = < u_i\dot{F}_{s,i} > -\widetilde{u_i}\widetilde{\dot{F}_{s,i}}$$

where the angled brackets stand for ensemble averaging over the droplets contained within the considered LES cell, and u_i is a corrected gas phase velocity, taking the subgrid fluctuations into account. This approach is described in section 2.4. These parameters are obtained by explicit modeling of the dispersed phase, as discussed below.

2.3 Dispersed Phase Modeling Assumptions

The present LES approach employs a Lagrangian approach,[17,20] since the ability to include droplet size effects (which directly impacts evaporation, fuel-air mixing and hence, combustion), is considered very important for accurate prediction. Solving for the particle evolution in space and time within the gas field can be computationally expensive if a large number of particles have to be tracked. Therefore, a sampling technique is employed, whereby characteristic groups of droplets are represented as "computational parcels". Each of these computational parcels represents a group of particles, all having identical size, location, velocity and temperature. For completeness, some of the assumptions used in the dispersed phase modeling are presented here, although more details can be found elsewhere.[18]

The spray field simulated here is assumed to be dilute. The dilute spray approximation implies that while particles interact with the gas phase, direct interaction between drops can be neglected. The dilute spray approximation also precludes the inclusion of droplet breakup effects and coalescence processes (which might be significant in a dense spray situation). This implies that the present model is not suitable for simulating the near field of the liquid atomizers/injectors where the droplet collisions are high.

The droplet is assumed to be spherical in this formulation. It is known that moving droplets tend to deform; however, the drag correlations (used in the present model) implicitly incorporate this effect and treats the droplets as equivalent spheres. The pressure at the location of the droplet is assumed to be constant during its interaction with the gas phase and equal to the local ambient pressure. This assumption is satisfactory, except at very low pressure. Diffusivities in the liquid and circulation velocity inside the droplet are assumed to be negligible. This is valid, when the size of the droplets are small (which is applicable for the present simulations). All external forces on the droplet such as, gravity, Coriolis, centrifugal, and Basset force, and virtual mass effect are neglected.[18] These approximations are valid, when the liquid-gas density ratio ($\rho_d/\rho >> 1$) is very high (which is valid here).

2.4 Equations for the dispersed phase

In modeling the spray field, it is assumed that the Kolmogorov scale is of the same order or larger than the largest droplets ($\approx 40\mu m$) in the spray field. For such a situation, the interaction between gas and liquid phases is dominated by laminar fluid dynamics. Given these assumptions, the governing equations for the dispersed phase, (following Oefelein and Yang[17]) are given by:

$$\frac{dx_{i,d}}{dt} = u_{i,d} \tag{8}$$

$$\frac{du_{i,d}}{dt} = \frac{3}{16}\frac{C_D \mu Re_d}{\rho_d r_d^2}(u_i - u_{i,d}) \tag{9}$$

Here, $u_{i,d}$ is the i-th component of the droplet velocity, ρ_d is the droplet density and r_d is the radius of the droplet. Re_d is the droplet Reynolds number defined as $Re_d = \sqrt{(u_i - u_{i,d})(u_i - u_{i,d})}d_d/\nu$, where C_D is the drag coefficient. The drag coefficient is obtained from empirical correlations for evaporating droplets (assuming that they retain the spherical shape). This results in the following expression for C_D:[18]

$$C_D = \begin{cases} \frac{24}{Re_d}(1 + \frac{1}{6}Re_d^{2/3}) & for \quad Re_d \leq 1000 \\ 0.424 & for \quad Re_d > 1000 \end{cases}$$

The effect of turbulence on the droplet motion is simulated using the Stochastic Separated Flow model.[18] The stochastic dispersion of droplets due to turbulent motion is incorporated by representing the gas phase velocity at particle location as $u_i = \tilde{u}_i + X\sqrt{2k^{sgs}/3}$, where X is a random number sampled from a uniform distribution (with zero mean). Note that, particles are not restricted to lie on the Eulerian grid points where the gas-phase properties are known. Therefore, an interpolation function S, of the following general form

$$\phi(x_d) = \sum_c S(x_d, x_c)\phi(x_c)$$

is used to estimate the gas phase properties at the particle location. Here, x_c is the Eulerian grid cell center and ϕ is any gas phase property known at the position x_c. An eight-point, volume-weighted averaging of the adjacent cells is used to interpolate the gas phase properties to the droplet locations, and also for the redistribution of the spray source terms from the particle position to the Eulerian grid (gas phase).

2.4.1 Droplet Mass Transfer:

The equation governing the mass conservation for the droplet is given by

$$\frac{dm_d}{dt} = -\dot{m}_d \tag{10}$$

where the mass of the particle is given by $m_d = (4/3)\pi r_d^3 \rho_d$ and $\dot{m}_d$ is the net mass transfer rate for a droplet in a convective flow field given by

$$\frac{\dot{m}_d}{\dot{m}_{Re_{d=0}}} = 1 + [0.278\sqrt{Re_d}Sc^{(1/3)}]/[1 + \frac{1.232}{Re_d Sc^{(4/3)}}]^{(1/2)}$$

Here, $Re_{d=0}$ is the Reynolds number for the droplet at rest. The governing equation for mass transfer under quiescent condition reduces to $\dot{m}_{Re_d=0} = 2\pi\rho_s D_{sm} d_d ln(1 + B_M)$ where ρ_s and D_{sm}, respectively, are the gas mixture density and the mixture diffusion coefficient at the droplet surface. Also, B_M is the Spalding number given by[19]

$$B_M = \frac{(Y_{fs} - Y_{f,\infty})}{(1 - Y_{fs})}$$

Here, Y_{fs} is the fuel mass fraction at the droplet surface, $Y_{f,\infty}$ is the fuel mass fraction in the ambient gas, and

$$Y_{fs} = \frac{X_{fs}W_f}{X_{fs}W_f + (1 - X_{fs})W_\alpha}$$

where W_α is the molecular weight of the gas (excluding fuel vapor), W_f is the molecular weight of the fuel and X_{fs} is the mole-fraction of the fuel at the droplet surface. The mole-fraction X_{fs} is obtained from the Raoult's law,[19] which assumes that the mole-fraction at the droplet surface is equal to the ratio of the partial pressure of the fuel vapor (p_{vp}) to the total pressure. For the present spray calculations, the partial pressure of the fuel vapor is computed based on the following empirical correlation[21]

$$ln(\frac{p_{vp}}{p_c}) = \frac{1}{(1 - x)}[P_{v_1}x + P_{v_2}x^{1.5} + P_{v_3}x^{2.5} + P_{v_4}x^5]$$

where $x = 1 - [T/T_c]$, and T_c and p_c are the critical temperature and critical pressure of the fuel vapor, respectively. The coefficients P_{v_1}, P_{v_2}, P_{v_3}, P_{v_4} for a given fuel vapor can be found elsewhere.[21]

2.4.2 Droplet Internal Temperature:

As a single droplet enters a hot environment, a small region of the droplet near the surface will heat up quickly while the central core of the droplet remains "cold". The heat conduction to its interior increases as the droplet penetrates further into the hot ambient gas. Eventually, the temperature within the droplet will become nearly uniform before the end of its lifetime. solving this transient phenomena within a droplet is not trivial, and various models have been proposed[18] of which the simplest is the uniform temperature model. In this model, the thermal conductivity is assumed infinite inside the liquid and therefore, the bulk liquid temperature is same as the surface temperature. However, the species mass fraction is allowed to be different from the bulk liquid and the ambient condition.

The equation governing the internal temperature distribution based on this uniform temperature model is

$$m_d C_{p,d} \frac{dT_d}{dt} = h_d \pi d_d^2 (\tilde{T} - T_d) - \dot{m}_d \Delta h_v$$

where Δh_v is the enthalpy of vaporization which is the energy required to vaporize one mole of liquid component into a gaseous mixture at a given temperature and pressure. Note that, this is not same as the latent heat of vaporization which represents the energy required to vaporize one mole of pure liquid in its own vapor at a given temperature and saturation pressure, $p_{sat}(T_d)$. The heat transfer coefficient, h_d for a droplet in a convective flow field with mass transfer is modeled following the proposed correlation of Faeth and Lazaar[22] :

$$\frac{h_d}{h_{Re_{d=0}}} = 1 + 0.278\sqrt{Re_d} Pr^{(1/3)} / [1 + \frac{1.232}{Re_d Pr^{(4/3)}}]^{1/2}$$

Here, the heat transfer coefficient at quiescent condition is $h_{Re_d=0} = Nu_{Re_d=0}\kappa/d_d$ where the $Nu_{Re_d=0}$ is the Nusselt's number at quiescent conditions given by $Nu_{Re_{d=0}} = 2ln(\alpha/\alpha - 1)$, where $\alpha = (1 + B_M)^{Le^{-1}}$ and Le is the Lewis number of the gas mixture evaluated using the Schmidt number and Prandtl number as $Le = Sc/Pr$.

2.5 Heptane/Air Chemistry

In order to simulate the heptane-air combustion, a single-step mechanism, developed by C.K. Westbrook and F.L. Dryer[23] is used. The global mechanism is described by:

$$C_7H_{16} + 11O_2 \rightarrow 7CO_2 + 8H_2O \qquad (11)$$

This reaction is assumed to follow an Arrhenius law, given by:

$$\dot{\omega}_{C_7H_{16}} = k_f [C_7H_{16}]^{0.25} [O_2]^{1.5}$$
$$k_f = 5.1x10^{11} exp(-\frac{15098}{T})$$

where k_f is in $\left(\frac{cm^3}{mol}\right)^{0.75} \frac{1}{s}$.

A conventional closure based on the subgrid Eddy Break-Up (EBU) model is employed. In this approach the filtered reaction rate is controlled by the turbulent timescales of the flow, corresponding to the subgrid scalar mixing rate. Reaction then occurs at the smallest of the time scale for mixing and reaction. The turbulent timescale was estimated by $\tau_{mix} = C_{EBU}\overline{\Delta}/\sqrt{2k^{sgs}}$.

3 Numerical Methods

The governing equations are solved using a finite-volume predictor-corrector scheme that is nominally second-order accurate in space and time. A fourth-order accurate scheme is also available but is not employed here. The central scheme used is not resistant to high-frequency oscillations appearing near shock-waves. In order to suppress spurious oscillations, a Total Variation Diminishing (TVD) type of artificial dissipation was added to the base scheme. The semi-discretized scheme takes the form:

$$\frac{d}{dt}\left(V_{ijk} U_{ijk}\right) + Q_{ijk} - D_{ijk} = 0$$

With $a_{i+1/2}$ the eigenvalue of the considered variable, and given the different quantities:

$$F_{i+1/2} = minmod(\Delta U_{i+1/2}, \Delta U_{i-1/2}) + minmod(\Delta U_{i+1/2}, \Delta U_{i+3/2}) - \Delta U_{i+1/2}$$

$$\lambda = \frac{\Delta t}{\Delta x}$$

$$\psi(z) = \begin{cases} |z| & for \quad |z| \geq \delta_1 \\ \frac{z^2+\delta_1^2}{2\delta_1} & for \quad |z| < \delta_1 \end{cases}$$

the dissipation term is computed as:

$$d_{i+1/2} = -\left[\psi(a_{i+1/2})\Delta U_{i+1/2} + \left(\lambda\beta(a_{i+1/2})^2 - \psi(a_{i+1/2})\right) F_{i+1/2}\right]$$

where $\beta = 1$. This TVD limiter corresponds to the explicit symmetric scheme of Davis.[24]

Fully supersonic (Dirichlet) conditions are imposed at the inflow, and supersonic outflow is used: extrapolation is applied for supersonic outflow (Neumann Boundary Conditions). Impermeable, slip wall boundary conditions are used for the top wall, while no-slip conditions are enforced along each side of the step, and at the bottom wall. Periodic boundaries are set for the spanwise direction.

4 Results and Discussion

4.1 Test case

As mentioned previously, the configuration chosen is identical to the research facility at WPAFRL.[11, 12, 8]

The free stream airflow has a total temperature of 950 K, a total pressure of 390 kPa, and a Mach number of 1.8.

For this study, only a small spanwise section of the combustor is studied. The cavity has a depth of $0.00207m$, an L/D ratio of 4.8, and an aft-ramp angle of 22 degrees. The domain of dimension $0.27m$ x $0.073m$ x $0.012m$ is discretized using 343x159x13 cells. A higher clustering of grid cells is employed close to the walls and in the shear layer. The computational grid is shown in Fig. 1.

To understand and to quantify the mixing of a given injection case two injection locations have been studied: (a) Injection on the step, 0.045m upstream the cavity leading edge, normal to the free stream, see Fig. 2 a), and (b) Injection from the cavity rear-wall, 0.002m below the step corner, at 45 degrees from the free stream, see Fig. 3 a). The first configuration is similar to the experimental setup.

For all the cases, the spray half angle is chosen to be 25 degrees, and the droplets have a constant radius of 25 μm. The velocity of the particles is also set at a constant value of 50 m/s.

4.2 Spray evaporation and fuel-air mixing

In the bottom wall injection case, the cold droplets are injected within the incoming boundary layer, where stagnation temperature is almost recovered. A high evaporation rate then takes place in the first period of the droplet lifetime. This blockage results in the creation of a weak shock, and a local separated region appears just upstream the spray injection point, as seen in Fig. 2 c).

Another consequence of the high initial evaporation rate is that the equivalence ratio peaks in the boundary layer, and these highly concentrated spots are convected downstream. Mixing takes place within the shear layer above the cavity, and consequently, as is apparent in Fig. 4, where equivalence ratio profiles along the cavity are shown, a mean equivalence ratio of 0.35 resides inside the cavity.

Simultaneously, the particles leave the hot boundary layer region, and penetrate into the free stream. The expansion due to the particles/gas coupling during the evaporation process results in the formation of a weak shock, a subsequent increase in static temperature and evaporation/mixing is thus enhanced in a second region, above the shear layer. This configuration shows interesting features for flame-holding capabilities: penetration of the fuel in the freestream is observed, while a significant amount of fuel is supplied to the cavity, so initiating reaction from the cavity heat reservoir to the freestream should be possible.

When the spray is injected directly into the cavity the particles are directly introduced into the hot pool formed by the cavity. A high evaporation rate is again observed at the beginning of the droplet lifetime. Indeed, the mean temperature in the cavity is close to the stagnation temperature of the incoming airflow. The angle of injection was chosen so that the particles quickly penetrate the freestream. Most of the evaporated fuel gets into the shear layer, and into the freestream.

As a consequence of this quick penetration in the airflow, very little gaseous fuel gets into the cavity, as can be seen in Fig. 4, where equivalence ratio profiles are compared to the bottom-wall injection configuration. The bottom wall injection case shows a better ability to increase the presence of the fuel in the free stream.

Injection inside the cavity results in a significant reduction of the "trapped vortex" size. The time-averaged vector field inside the cavity is shown in Fig. 5 for the non-injecting configuration, and in Fig. 3 c) for the cavity injection. Without injection, the vortex diameter is about the cavity depth, whereas with injection inside the cavity, the vortex is compressed along the lower wall of the cavity, and very little interaction with the shear layer is observed.

4.3 Turbulent motion and flow dynamics

Profiles of the LES resolved axial turbulence intensity $\overline{u'u'}$ and Reynolds stress $\overline{u'v'}$ are shown in Figs. 6 and 7, respectively for a base case without injection (reference case), and for both the bottom-wall and cavity injection configurations.

The reference case shows a peak in axial turbulence intensity emerging from the boundary layer on the step, that grows in the shear layer formed above the cavity. The anisotropic part shows the same trend. The effect of the bottom wall injection on the turbulent motions is to increase significantly these turbulent levels all along the shear layer. Also, a significant amount of turbulence is added to the freestream, which seems to diffuse as convected downstream.

A very high level of turbulence is generated along the ramp of the cavity. The flow dynamics show a small amplitude flapping of the shear layer, that periodically impinges on the aft-ramp, and results in mass entrainment from the cavity into the freestream. A sequence of numerical shadowgraph pictures of the flowfield is shown in Fig. 8, where the part of the shear layer close to the cavity trailing-edge is observed to flap. The freestream motion (i.e., the shock location and motion) as well as the cavity flow are affected during this process.

In the case of cavity injection, it is seen that the level of $\overline{u'u'}$ is slightly increased in the shear layer region, and that a new peak of turbulence appears in the freestream, in the wake of the spray. However, the anisotropic part is not much affected by the spray. In general, regions of gradient and counter-gradient transport (in the mean sense) are seen in the $\overline{u'v'}$ at the edges of the shear layer and in the cavity. In con-

trast, a conventional RANS approach will impose a gradient transport closure at all locations and thereby fail to capture the counter-gradient effect.

4.4 Combustion results

Injection was set at the bottom wall only, in a similar manner to the mixing configuration described previously. The global equivalence ratio, based on a total evaporation of the droplets assumption, was 0.92.

4.4.1 Ignition

In order to initiate combustion in the experiments, Mathur *et al*[8] used an air throttle downstream of the cavity in order to generate a pre-combustion shock train that facilitates ignition of the liquid fuel in the combustor. Turning the air throttle off would lead to a stable and continuous combustion if the heat release was high enough.

A hot environment is indeed necessary for a fast evaporation of the droplets to occur, and a fast evaporation is in turn necessary for a high heat release to take place. Ignition of a supersonic dual-phase system is a critical issue.

In this simulation, a few ignition approaches have been tested. The use of an instantaneous infinite-rate chemistry was first tested. This approach resulted in hot regions along the jet path which enhanced the evaporation. However, mixing was not achieved, and reaction would not stabilize. The use of infinite-rate on a longer simulation time was not found to be efficient either. The waves generated by this method would disturb significantly the flow.

The approach adopted was then to let the mixing timescale dominate the chemistry in the EBU approach for a simulation time of one flow through time. A smooth ignition was then reached.

4.4.2 Bottom wall injection

After ignition continuous combustion could be reached by adjusting the C_{EBU}, defined in section 2.5, to a value lower than unity (0.1). Temperature, CO_2 and vorticity fields are shown in Fig. 9.

A reverse flow is observed at the edge of the step, that brings hot products upstream the cavity. Comparison of velocity profiles for reacting and non-reacting cases is shown in Fig 10. The reverse flow is identified at the edge of the step, and the re-circulation region appears to extend further into the freestream when reaction occurs. Higher levels of kinetic energy are observed inside the cavity when the flow is reacting.

The boundary layer, fuel-rich, separates due to the reverse flow, and reaction is initiated in this separated region. The droplets penetrate the hot shear layer, and evaporate. Part of the reaction products get into the cavity.

The shock created by the injection and by the separation of the boundary layer reflects on the top wall of the combustor, and bends the shear layer down. The reaction zone is then confined in the lower part of the domain. Moreover, only 40% of the droplets is evaporated at the domain outflow.

Overall, a poor efficiency is observed for this configuration. The dynamics of the flow prevent the combustion zone from extending up to the upper wall of the combustor, and the droplets are partly evaporated only when they leave the domain. A better mixing between air and fuel should then be achieved when injection is done both at the top and bottom walls.

5 Conclusion

A numerical study of a dual-phase model SCRAMJET engine was carried out. Two injection options have been compared in terms of species mixing, turbulence generation and flow dynamics. The most suitable to flame-holding, injector on the bottom wall, upstream the cavity, was then ignited, and combustion characteristics were identified. The lack in efficiency of a single injector configuration was pointed out.

The current LES approach shows good capturing of the flow features. A better simulation of the spray mixing and combustion could however be achieved by using more sophisticated subgrid mixing modeling, and more detailed finite-rate kinetics. The Linear Eddy Model (LEM) was shown to be an accurate and powerful mixing model, and very good prediction for mixing[25] and combustion[26] in supersonic flows were reached using this approach.

Acknowledgments

This work is supported by NASA University Institute at University of Florida under grant NCC3-994.

References

[1]Owens, M. G., Tehranian, S., Segal, C., and Vinogradov, V., "Flame-Holding Configurations for Kerosene Combustion in a Mach 1.8 Airflow," *Journal of Propulsion and Power*, Vol. 17, No. 4, pp. 456–461.

[2]Curran, E. T. and Murthy, S. N. B., "SCRAMJET Propulsion," *Progress in Astronautics and Aeronautics*, Vol. 189, 2000, pp. 13–17.

[3]Waltrup, J. P., "Upper Bounds on the Flight Speed of Hydrocarbon-Fueled Scramjet-Powered Vehicles," *Journal of Propulsion and Power*, Vol. 17, No. 6, 2001, pp. 1199–1204.

[4]Papamoschou, D. and Roshko, A., "The compressible turbulent shear layer:an experimental study," *Journal of Fluid Mechanics*, Vol. 197, 1998, pp. 453–477.

[5]Yu, K., Kraeutle, K. H., Wilson, K. J., Parr, T. P., and Smith, R. A., "Supersonic flow mixing and combustion using ramp nozzle," *AIAA Paper 92-3840*, 1992.

[6]Fernando, E. M. and Menon, S., "Mixing Enhancement in Compressible Mixing Layers: An Experimental Study," *AIAA Journal*, Vol. 31, No. 2, 1993.

[7]Kumar, A., Bushnell, D. M., and Hussaini, M. Y., "A Mixing Augmentation Technique for Hypervelocity Scramjets," *AIAA Paper 87-1882*, 1987.

[8]Mathur, T., Lin, K.-C., Kennedy, P., Gruber, M., Donbar, J., Jackson, T., and Billig, F., "Liquid JP-7 Combustion in a Scramjet Combustor." *AIAA Paper 2000–3581*, 2000.

[9]Rogallo, R. S. and Moin, P., "Numerical Simulation of Turbulent Flows," *Annual Review of Fluid Mechanics*, Vol. 66, 1984, pp. 99–137.

[10]Lesieur, M., "Recent Developments in LES of Turbulence," *New Tools in Turbulence Modelling*, edited by O. Metais and J. Ferziger, Springer-Les Editions De Physique, 1996, p. 222.

[11]Jackson, K., Gruber, M., Mathur, T., Streby, G., Smith, C., and Billig, F., "Calibration of a Newly Developed Direct-Connect High-Enthalpy Supersonic Combustion Research Facility." *AIAA Paper 98–1510*, 1998.

[12]Gruber, M., Baurle, R., Mathur, T., and Hsu, K.-Y., "Fundamental Studies of Cavity-Based Flameholder Concepts for Supersonic Combustors." *AIAA Paper 99–2248*, 1999.

[13]Kim, W.-W., Menon, S., and Mongia, H. C., "Large Eddy Simulations of a Gas Turbine Combustor Flow," *Combustion Science and Technology*, Vol. 143, 1999, pp. 25–62.

[14]Chakravarthy, V. and Menon, S., "Large-Eddy Simulations of Turbulent Premixed Flames in the Flamelet Regime," *Combustion Science and Technology*, Vol. 162, 2001, pp. 175–222.

[15]Kim, W.-W. and Menon, S., "A New In-compressible Solver for Large-Eddy Simulations," *International Journal of Numerical Fluid Mechanics*, Vol. 31, 1999, pp. 983–1017.

[16]Sankaran, V. and Menon, S., "LES of Scalar mixing in supersonic mixing layers," *Submitted to : Proceedings of the Combustion Institute*, Vol. 30, 2004.

[17]Oefelein, J. C. and Yang, V., "Analysis of transcritical spray phenomena in turbulent mixing layers," *AIAA 96-0085, 34th AIAA Aerospace Sciences Meeting*, 1996.

[18]Faeth, G. M., "Mixing, transport and combustion in sprays," *Progress in Energy and Combustion Science*, Vol. 13, 1987, pp. 293–345.

[19]Chen, K. H. and Shuen, J. S., "A coupled Multi-block solution procedure for spray combustion in complex geometries," *AIAA-93-0108, 31st AIAA Aerospace Sciences Meeting*, 1993.

[20]Pannala, S. and Menon, S., "Large eddy simulations of two-phase turbulent flows," *AIAA 98-0163, 36th AIAA Aerospace Sciences Meeting*, 1998.

[21]Reid, R. C., Prausniz, J. M., and Poling, B. E., *The properties of gases and liquids*, Mcgraw Hill Publishing Co.,, 1988.

[22]Faeth, G. M. and Lazar, R. S., "Fuel Droplet burning rates in a combustion gas environment," *AIAA Journal*, Vol. 9, 1971, pp. 2165–2171.

[23]Westbrook, C. K. and Dryer, F. L., "Simplified Reaction Mechanisms for the Oxidation of Hydrocarbon Fuels in Flames," *Combustion Science and Technology*, Vol. 27, 1981, pp. 31–43.

[24]Davis, S. F., "TVD Finite Difference and Artificial Viscosity," *ICASE report No. 84 - 20*, 1984.

[25]Sankaran, V., Génin, F., and Menon, S., "A Sub-Grid Mixing Model for Large Eddy Simulation of Supersonic Combustion." *AIAA Paper 2004–0801*, 2004.

[26]Génin, F., Chernyavsky, B., and Menon, S., "Large Eddy Simulation of Scramjet Combustion Using a Subgrid Mixing/Combustion Model." *AIAA Paper 2003–7035*, 2003.

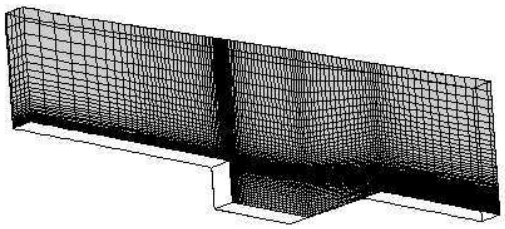

Fig. 1 Computational grid.

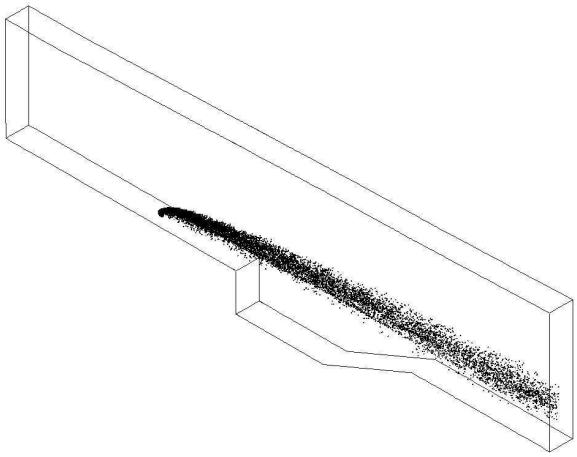

a) spray penetration.

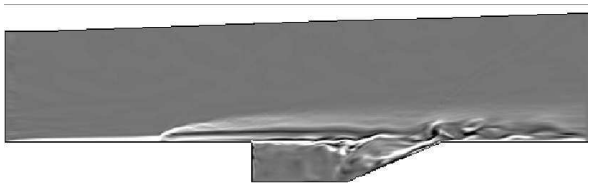

b) Instantaneous Z-vorticity contours.

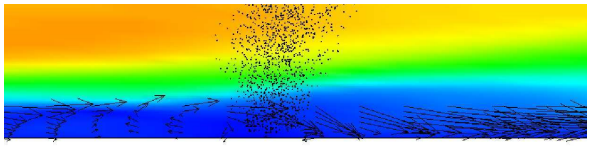

c) Vector field in the injection area.

Fig. 2 Flowfield for bottom wall injection.

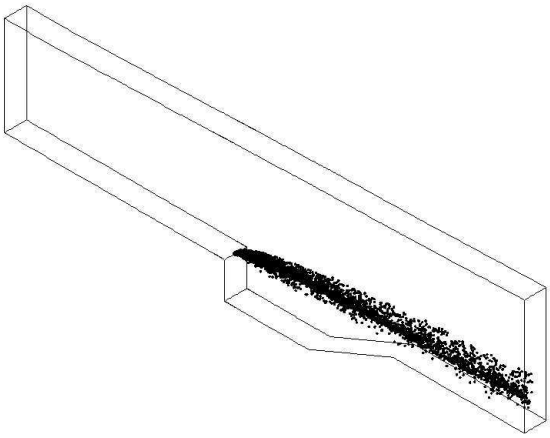

a) spray penetration.

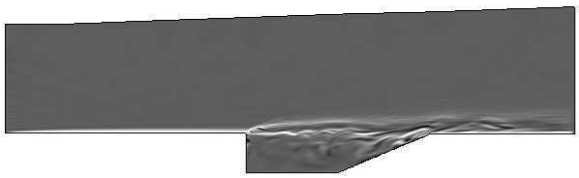

b) Instantaneous Z-vorticity contours.

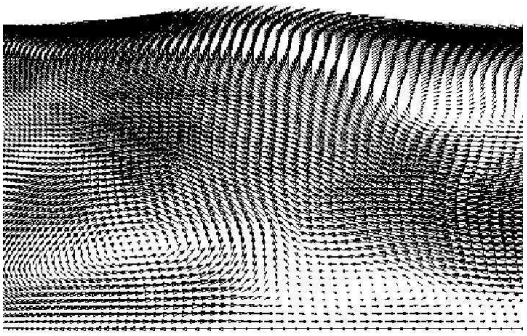

c) Vector field in the injection area.

Fig. 3 Flowfield for cavity injection.

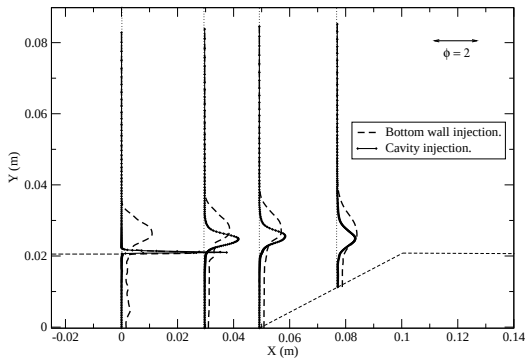

Fig. 4 Equivalence Ratio profiles at four locations along the cavity.

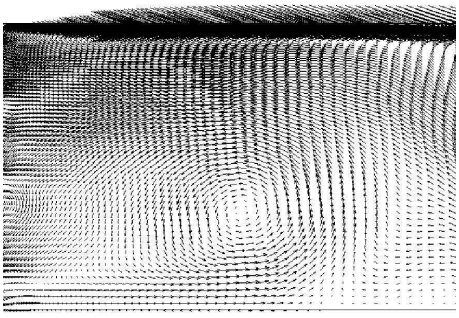

Fig. 5 Trapped vortex - No injection.

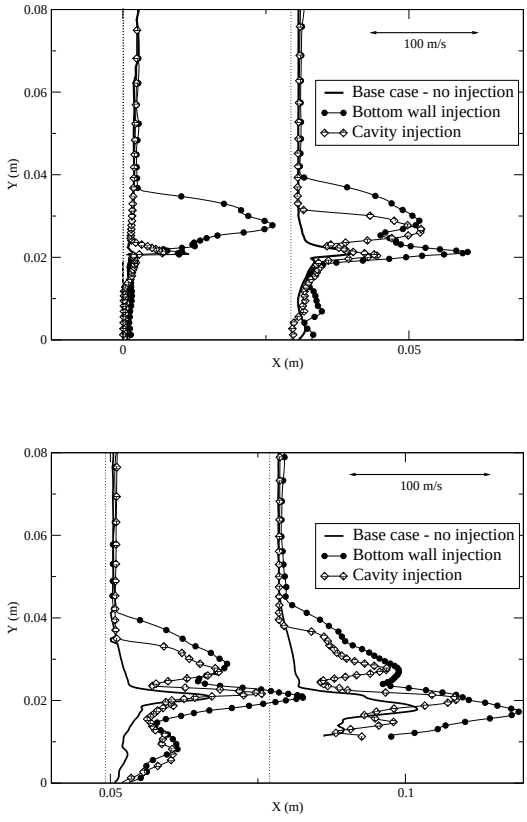

b)

Fig. 6 $\overline{u'u'}$ profile at four locations: a) X=0.m and X=0.029m b) X=0.049m and X=0.077m.

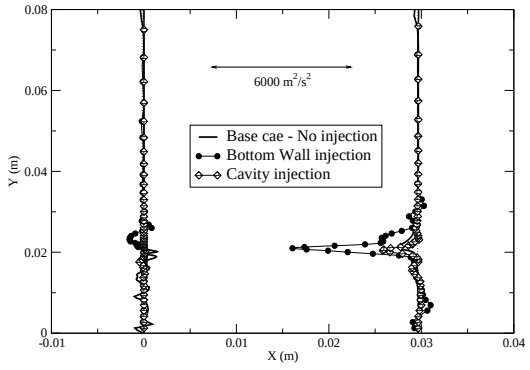

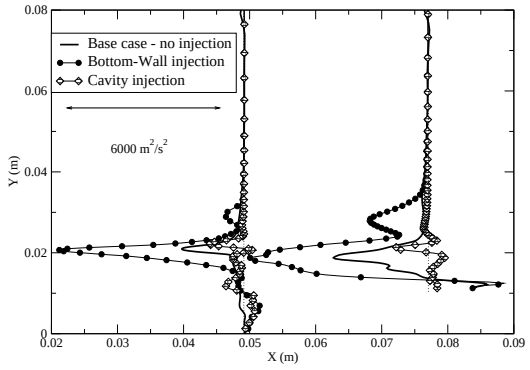

b)

Fig. 7 $\overline{u'v'}$ **profile at four locations: a) X=0.m and X=0.029m b) X=0.049m and X=0.077m.**

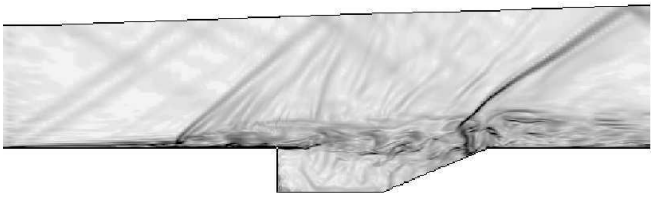

a)

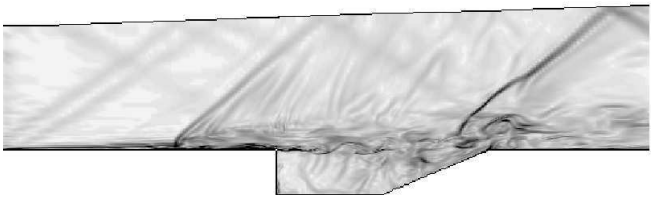

b)

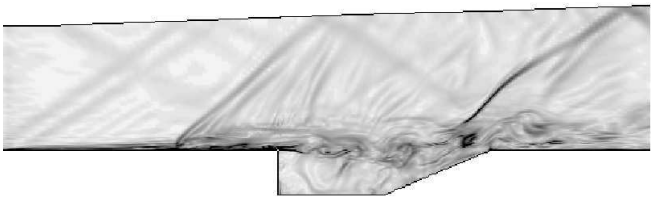

c)

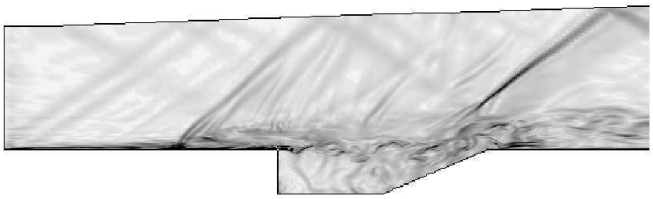

d)

Fig. 8 Snapshots of the density gradient field.

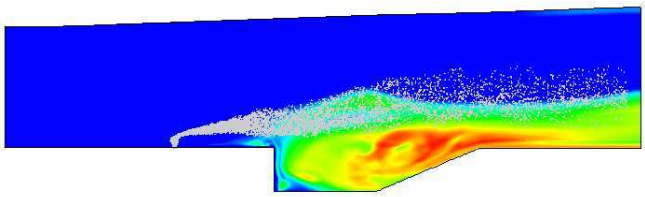

a) Temperature field

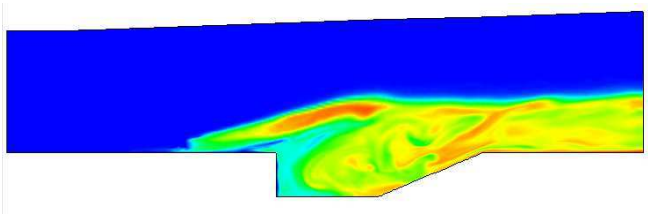

b) CO_2 field

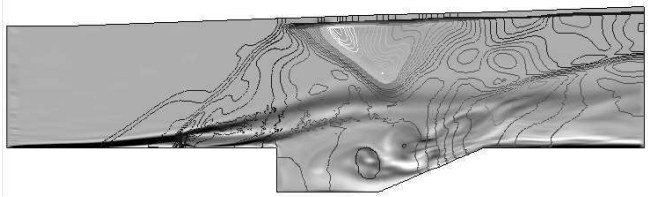

c) Z-vorticity field, pressure contours

Fig. 9 Instantaneous flowfields for the reacting system, bottom wall injection

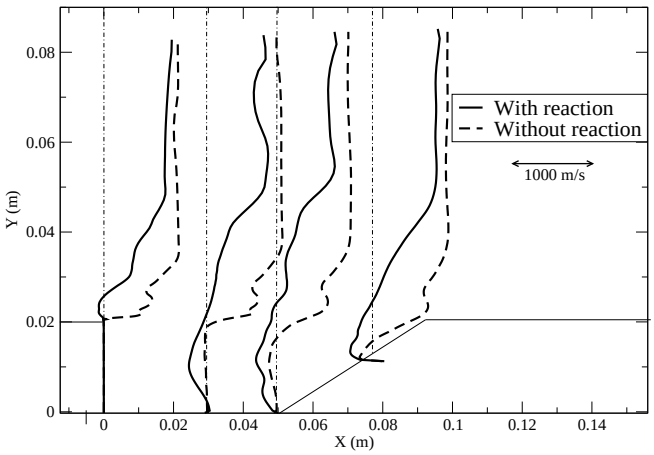

Fig. 10 Velocity profiles along the cavity.